Published in final edited form as:
*Acad Radiol*. 2009 June ; 16(6): 718–725. doi:10.1016/j.acra.2008.12.003.

# Volumetric Xenon-CT Imaging of Conventional and High-Frequency Oscillatory Ventilation

**Daniel G. Mulreany, BS**[1], **Brett A. Simon, MD, PhD**[1,2], **Kieran J. Murphy, MD**[3], and **R. Blaine Easley, MD**[1,4]

[1]Department of Anesthesiology and Critical Care Medicine, The Johns Hopkins University Baltimore, MD

[2]Department of Medicine, The Johns Hopkins University Baltimore, MD

[3]Department of Radiology, The Johns Hopkins University Baltimore, MD

[4]Department of Pediatrics, The Johns Hopkins University Baltimore, MD

## Abstract

**Rationale and Objectives—**For mechanical ventilation of patients with pulmonary injuries it has been proposed that high-frequency oscillatory ventilation (HFOV) offers advantages over conventional ventilation (CV), however, these advantages have been difficult to quantify. We used volumetric, dynamic imaging of Xenon (Xe) washout of the canine lung during both HFOV and CV to compare regional ventilation in the two modalities.

**Materials and Methods—**Three anesthetized, mechanically ventilated animals were studied, each at three different ventilator settings. Imaging was performed on an experimental Toshiba 256-slice scanner at 80 kV, 250 mAs, and 0.5 sec scans, yielding 12.8 cm of Z-axis coverage. Repeated images were acquired at increasing intervals between 1 and 10 seconds for 90 seconds during HFOV, and using retrospective respiratory gating to end-expiration for 60 seconds during CV.

Image series were analyzed to quantify regional specific ventilation ($sV̇$) from the regional density washout time constants.

**Results—**High quality, high-resolution regional ventilation maps were obtained during both CV and HFOV. Overall ventilation decreased at smaller tidal volume, as expected. Regional $sV̇$ was more uniform during HFOV compared to CV but the underlying distribution of lung aeration was similar.

**Conclusions—**High-resolution volumetric ventilation maps of the lung may be obtained with the 256-slice multidetector CT scanner. There is a marked difference in the distribution of regional ventilation between CV and HFOV, with a significant gravitational ventilation gradient in CV that was not present during HFOV. This technique may be useful in exploring the mechanisms by which HFOV improves gas exchange.

### Keywords

regional ventilation; computed tomography; mechanical ventilation; gas exchange; canine



Address correspondence to: Brett A. Simon, MD, PhD Dept. of Anesthesia, Tower 711 600 N. Wolfe St. Baltimore, MD 21287−8711 (410) 614−1515 / (410) 955−0994 FAX E-mail: bsimon@jhmi.edu.

## INTRODUCTION

Functional lung imaging with X-ray computed tomography (CT) facilitates the study of pulmonary structure-function relationships by providing both detailed anatomic information as well as co-localized physiologic information (1,2). As the speed and volumetric coverage of multi-detector CT (MDCT) scanners has increased over time, so has the ability to rapidly and efficiently characterize variation in regional lung function across the entire lung. Recently, volumetric CT image acquisition took a giant leap with the introduction of the Toshiba Aquilion One scanner, an MDCT scanner capable of acquiring 320 contiguous 0.5mm thick axial slices in a single 0.33 sec rotation, making true volumetric CT imaging commercially available. We had an opportunity to test a pre-production 256 slice version of this scanner to evaluate its potential for studying the distribution of pulmonary gas exchange during high-frequency oscillatory ventilation (HFOV), a novel form of mechanical ventilation with application in management of patients with refractory acute lung injury (3).

For mechanical ventilation of patients with pulmonary injuries, it has been proposed that HFOV offers advantages over conventional ventilation (CV), however, the physiology of HFOV remains poorly characterized (3,4). In contrast to CV, which delivers breaths that mimic normal breathing with volumes of 400−900 ml at 6−30 breaths/minute, HFOV delivers breaths of 40 −150 ml at 180−900 breaths/minute (3−15 Hz). The rationale behind this approach is that by ventilating with smaller breaths about an elevated mean lung volume, it may be possible to avoid the injurious extremes of lung overdistention and collapse which can arise from the large volume excursions applied to the stiff, injured lung during CV (3). Because the tidal volume in HFOV is smaller than the anatomic dead space (the volume of the conducting airways leading to the gas-exchanging alveolar region), the methods of gas exchange and, further, the factors governing the distribution of ventilation, are distinctly different from those in CV. It has been difficult to directly measure these differences in intact subjects.

We used volumetric, dynamic computed tomography (CT) imaging of Xenon (Xe) washout from the canine lung during both HFOV and CV in order to compare regional ventilation distributions in the two modalities. This Xe-CT method measures regional ventilation from the washout rate of the radiodense gas Xe, determined from the changing density of the lung parenchyma in serial CT images as dense resident Xe gas is replaced with air during successive breaths (5,6). By applying this technique on the new volumetric CT scanner, ventilation can be determined for the majority of the lung volume with high spatial resolution in a single imaging run, a result that could previously only be approximated by combining multiple Xe washout studies with incremental table movement, a procedure that is both time and radiation exposure intensive as well as being prohibitively expensive.

Because we were using a pre-clinical, test model Toshiba scanner and image reconstruction was performed off-line, we were limited in the number of imaging runs we could perform in a single study. For this reason the study was designed as a small pilot to investigate the feasibility of performing and analyzing volumetric Xe-CT studies during HFOV. However, the results showed not only that high-resolution ventilation maps of the lung could be obtained but that there were significant and unanticipated differences in ventilation distribution between CV and HFOV that, if confirmed, could impact the way in which HFOV is used in critically ill patients.

# METHOD AND MATERIALS

## Animal Preparation

The animal protocol was approved by the institutionals Animal Care and Use Committee. Three mongrel dogs (19.3 ± 1.2 kg) were anesthetized (pentobarbital 25 mg/kg i.v. initially and 10 mg/kg i.v. hourly) and orally intubated with a 9.0 mm cuffed endotracheal tube. Muscle relaxation was provided with pancuronium (0.1 mg/kg i.v. initial and 0.05 mg/kg i.v. as needed). Dogs were also instrumented with a percutaneous femoral arterial catheter placed under sterile conditions for blood pressure monitoring and arterial blood gas sampling. All animals had arterial oxygen saturation ($SaO_2$) monitored with a pulse oximeter applied to the tongue (Nellcor N100). Initial mechanical CV settings were established with a Draeger Evita 2 Dura ventilator (Draeger Medical, Lübeck Germany) using room air at a respiratory rate (RR) of 16 breaths/minute and tidal volume (Vt) adjusted to produce an end-tidal partial pressure of $CO_2$ ($ETPCO_2$) of 30−35 mmHg. Subsequent ventilator settings for imaging were as noted below. Arterial blood gas measurements were made on a Chiron 855 Blood Gas Analyzer (Chiron Inc., Emeryville, CA). All measurements were performed in the supine position. At the conclusion of each study, the muscle relaxant was reversed with neostigmine and atropine (2 mg and 1 mg i.v.), the animals emerged from the anesthesia and extubated. All animals recovered uneventfully.

HFOV was provided with a custom-built piston ventilator (7) that provided closed-loop control of piston displacement independent of gas composition. Mean airway pressure was regulated by the computer-controlled balancing of the inflow and outflow of a 10 l/min bias flow with mass flow controllers (Sierra Instruments, Model 840, Monterey, CA). The software implemented (LabView 7, National Instruments, Austin, TX) control system automatically compensated for the changing density as the bias flow gas was changed from Xe to air. For each subject, the HFOV Vt required for eucapnia at settings of oscillatory frequency ($f$)=10 Hz, mean airway pressure (MAP)=10 cm $H_2O$, and inspiratory:expiratory ratio=1:1, was determined in the laboratory prior to transport to the imaging suite.

## Experimental protocol

As the purpose of this study was to demonstrate the feasibility of volumetric Xe-CT ventilation scanning during CV and HFOV, secondly because a limited number of imaging runs could be performed on this experimental scanner, and lastly because image reconstruction and analysis needed to be performed off-line, a range of ventilator settings were arbitrarily chosen that we anticipated would demonstrate measurable changes in both total ventilation and ventilation distribution (Table 1). Initially, we planned only to study HFOV (animal 1). For animal 2, a mechanical failure of the HFO ventilator occurred just as imaging was about to commence and thus only CV imaging could be performed. Finally, we recognized that there appeared to be differences in ventilation distribution between animals 1 and 2, so we studied both modes in animal 3 to distinguish an effect of ventilation mode from subject characteristics. In each case, the animal was anesthetized and instrumented in the laboratory, baseline ventilator settings determined, and then transported anesthetized to the imaging suite. Ventilation and monitoring was reestablished and imaging performed as described below.

## Imaging

Imaging was performed on a pre-clinical experimental Toshiba 256-slice Computed Tomography (CT) scanner. All images for each of the three dogs were acquired under the following settings. 256−0.5mm thick slices were acquired for each spin of the gantry, yielding 12.8 cm of Z-axis coverage (Figure 1 illustrates Z-axis coverage vs. 16 and 64 slice scanners). For all scans, settings were: 80 kVp, 125 mAs, 0.5 second scan time, 240 mm FOV, and 0.468x0.468x0.5 mm voxel size. Whole lung volume images were first obtained during a

breathhold, with large displacement table movement used to "stitch" together three overlapping lung volumes. The table position was then fixed so that the dynamic images of tracer washout were obtained over a single volume extending from above the diaphragm, chosen to allow simultaneous comparison of both apex and base regions. The Xe-CT washout images were acquired continuously during ventilation and retrospectively gated to reconstruct only those images from the desired time points (see below). While scout and rough axial images could be viewed immediately, final image reconstruction and gating was performed offline. A newly devised algorithm, coined ConeXact, was developed by Toshiba specifically to overcome the cone-beam artifact associated with such a large detector array and resulted in a small loss of image from the periphery of the end slices.

Prior to each imaging run, the animals were ventilated at the desired CV or HFOV settings for 15 minutes. The inspired gas was then switched to a mixture of approximately 40−60% Xe (balance $O_2$) from a 100 liter Douglas bag for 5 minutes to equilibrate the mixture throughout the lungs. Three images were acquired as an equilibrated baseline and then the inspired gas was switched from Xe to air. Repeated images were acquired as the Xe was washed out of the lung. During HFOV, in which respiratory period (0.1 sec) is much shorter than the 0.5 sec imaging time and there is minimal lung motion, 20 images were obtained using retrospective gating at fixed increasing intervals between 1 and 10 seconds over a period of 90 seconds. This scheme was used in order to insure adequate sampling of both fast and slow time constant lung regions. During CV, in which there are large lung volume changes during each tidal breath, 30 images were retrospectively gated to end-expiration so that each image was obtained at the same lung volume.

### Image Analysis

Image series were analyzed with software developed by the Iowa Comprehensive Lung Imaging Center (Division of Physiologic Imaging, Department of Radiology, Univ. of Iowa, Iowa City, IA) to quantify regional ventilation from the regional density washout time constants (5,8). Images were divided into regions of interest (ROI's) chosen to be 8 voxels high, 8 voxels wide, and 4 slices thick (3.5 mm, 3.5 mm × 2mm) as a balance between spatial resolution, analysis workload, and noise. For every ROI, the density at each of the 20−30 time points over the course of the study was measured and a nonlinear curve fitting process used to fit an exponential to its time-density curve. Voxels were not filtered for density range prior to processing, but curve fits were required to have a normalized summed squared residual below 100 to be included. Figure 2 illustrates the curve-fitting process for two individual ROIs. With the assumption that the tissue volume remains constant for a given ROI over the short period of the scan time, the exponential time constant of the washout curve is inversely proportional to the alveolar ventilation per unit alveolar volume (specific ventilation, $s\dot{V}$, units: 1/min), allowing regional ventilation to be quantified on a very fine spatial scale.

The volumetric lung washout image series were analyzed slice by slice and then output as a 3-dimensional map of $s\dot{V}$ for the entire scanned volume of lung (Figure 3). These data may be color-coded for visualization (Figure 4), as well as the ventilation distributions quantitatively analyzed (Table 2).

## RESULTS

Volumetric Xe-CT ventilation maps were successfully generated for each of the three animals under three ventilator settings. Minimal to no motion artifact was observed in the ungated HFOV images, but there was occasionally some slow variation in lung volume (and thus density) over time related to small oscillations in mean airway pressure from the bias flow control system (Figure 2). Approximately 50−100 HU of density enhancement was obtained from the Xe concentrations achieved. For display purposes the ventilation maps are presented

in a 2-dimensional format by averaging every 1.8 cm of z-coverage into one 2D colormap, creating six 2D maps which represent the entire scanned volume from apex to base (Figure 3).

Ventilation maps for subject 2 during CV at two tidal volumes are presented in Figure 4 and demonstrate the previously reported characteristic vertical gradient of ventilation in the Y-axis (dorsal-ventral), with more ventilation in the dependant/dorsal areas and less in the non-dependant/ventral areas (6,9). In addition, the shift in color towards yellow/red indicated increased overall ventilation with increased tidal volume. A similar vertical gradient in ventilation during CV is evident in the ventilation maps from subject 3 (Figure 5, bottom row). During HFOV, however, ventilation was extremely uniform and no vertical gradient is seen (Figure 5, upper two rows). There is an increase in average ventilation as Vt increased during HFOV (Figure 5). For comparison, corresponding maps of lung density distribution (Figure 6) for these same three ventilation settings are nearly indistinguishable, demonstrating that the distribution of air volume is unchanged in HFOV and therefore the ventilation changes are not a result of lung aeration or regional compliance differences (8). A similar uniform pattern of ventilation during HFOV was observed in subject 1 (data not shown).

The contribution of the vertical ventilation gradients to overall ventilation heterogeneity was estimated by stepwise multiple linear regression (6) and also examination of the coefficient of variation (Table 2). For the regression analysis, $s\dot{V}$ was used as the dependent variable and vertical height (Y), side (S, left vs. right), and coronal location (Z, apex-base) as independent variables. The means and standard deviations for $R^2$ as each independent variable was added are presented in Table 2. During CV, the vertical gradient accounted for 29% of the variance, with no additional improvement in the correlation coefficient $R^2$ with the addition of the other variables. In contrast, during HFOV less than 3% of the variance could be explained by the vertical gradient, with less than 5% explained by all the topographic parameters, indicating a very uniform distribution of ventilation. In addition, we compared the coefficient of variation (COV) of the $s\dot{V}$ data in each mode. This total COV ($COV_t$) is calculated as the ratio of the standard deviation of each data set to its mean and is a measure of dispersion. When applied to the $s\dot{V}$ data it is a measure of the heterogeneity of ventilation across conditions. In addition to looking at the total heterogeneity of ventilation, we can remove the influence of a dorsal-ventral or vertical ventilation gradient by subtracting from each voxel the average $s\dot{V}$ for all voxels at that vertical height and then recomputing the COV. This new $COV_i$ value quantifies the intrinsic ventilatory heterogeneity present in the lung that is not accounted for by a vertical gradient. The residual $COV_y$, calculated from the relationship $(COV_t)^2=(COV_i)^2 + (COV_y)^2$, gives the amount of heterogeneity attributable to the vertical gradient. Table 1 shows that while the total heterogeneity during CV was greater than during HFOV, this difference was due to the heterogeneity introduced by the vertical ventilation gradient seen in CV ($p<0.001$ $COV_y$ CV vs. HFOV).

## DISCUSSION

The availability of high-speed, high-resolution volumetric CT imaging of the lung has been the holy grail for the study of pulmonary structure-function relationships in intact subjects. In the early 1980s the dynamic spatial reconstructor, a one-of-a-kind volumetric scanner consisting of 14 rotating x-ray sources and detectors that could obtain 240−0.9mm thick axial images in 1/60 sec, showed the potential of such a system and led to several important physiologic insights including how regional lung expansion changes with posture, heart-lung interactions, and pulmonary vascular accommodations to chronic pressure loads (10-14). Conventional CT has been slow to catch up, but the recently released 320- slice Toshiba Aquilion One CT scanner comes close, acquiring up to 16 cm of 0.5mm thick contiguous axial slices with each 0.35 sec spin of the gantry. In addition to the simultaneous multislice image acquisition removing registration errors and reducing motion artifact, these technologies permit

the multi-scan study of dynamic temporal events, such as lung emptying and tissue deformation (2) and, with the use of inhaled or injected contrast agents, ventilation and perfusion (15). However, these extremely large image sets present significant challenges with respect to data management and processing, and the increased information from higher resolution must be balanced against noise, storage, and workload so that analysis proceeds on a scale appropriate to the questions asked.

The Xe-CT method provides for the non-invasive, high-resolution measurement of regional ventilation in intact subjects and has a number of previously described limitations (16). Briefly, the method requires the inhalation of non-radioactive Xe gas, which has anesthetic side-effects that limit the concentration that can be used in humans (17). Xe is significantly denser than air and thus its intrapulmonary distribution may differ slightly from normal breathing (5). In addition, the method requires repeat CT imaging of the lung to determine the regional washin and/or washout time constant over several breaths, entailing increased radiation exposure compared to single breath techniques (8) and magnetic resonance imaging. However, Xe-CT has the significant advantage of simultaneously providing high spatial resolution anatomic images, which combined with novel CT techniques for measuring regional perfusion (18) and sub-voxel texture (19,20), allows the comprehensive quantitative characterization of lung structure and function (21).

Applying the Xe-CT method to high-frequency oscillatory ventilation presented several challenges. Since HFOV utilizes very small tidal volumes at high rates, there is minimal lung motion. Lung volume is controlled by an electronic system that balances the inflow and outflow of fresh gas in a closed system to regulate mean airway pressure while also providing oxygen and eliminating $CO_2$. Switching this bias flow between air and the much denser $Xe/O_2$ mixture required development of a control system that was unperturbed by the effective variable gain introduced when the denser gas mixture passed through the mass flow controllers. To simplify this process, and because we did not know in advance the optimal timing for image acquisition during HFOV, we opted to only study the washout of Xe from the lung after steady state equilibration. While there are potential improvements in signal:noise ratios with the washin-washout procedure (22), there are recent data to suggest washin and washout time constants may differ under certain conditions during conventional ventilation (5). Furthermore, we used a simple large volume closed circuit reservoir system, without tight control of Xe concentration, for Xe equilibration. This system resulted in some variation in the final equilibration Xe concentration, which does not effect the calculation of the washout time constants but will reduce signal:noise at lower concentration (17). Because there is minimal lung motion during HFOV, respiratory gating of images is not necessary and we could arbitrarily image at increasing time intervals during the washout to insure that a wide range of time constants would be appropriately sampled.

Although limited by the number of image sets we could acquire by the pilot nature of this study in a test CT scanner, we were able to make several interesting observations. First of all, we were successful in creating high quality, high-resolution ventilation maps on nearly the entire lung with each imaging run (Figure 3). During CV, the overall ventilation varied quantitatively with changes in ventilator settings and exhibited the expected vertical gradient in regional ventilation in the supine position (Figure 4) previously described using several techniques (6, 9,23,24). This gravitational ventilation gradient has been ascribed to a parallel vertical gradient in lung expansion caused by a number of factors including the vertical gradient in pleural pressure, the weight of the heart on the left lung, and the shape and effect of the diaphragm compressing the lung base, all of which result in the more dependent lung tissue being relatively less expanded (Figure 6) and more compliant than the non-dependent tissue. The more compliant lung regions therefore receive a greater relative tidal volume.

During HFOV, however, ventilation was remarkably uniform (Figure 5), although the vertical gradient in lung aeration seen during CV was unchanged during HFOV (Figure 6) so that regional compliance cannot explain this observation. There are limited data in the literature for direct comparison. Yamada and colleagues (25) used PET imaging to study ventilation distribution during HFOV and also found a reduced dependent/non-dependent ventilation ratio at higher HFOV frequency, although they also observed relatively increased ventilation to base and central regions that were still present at 9 Hz but somewhat reduced compared to lower oscillation frequencies. Allen et al. measured alveolar pressure oscillations during HFOV in open-chest animals and also found an increased amplitude in the base as frequency increased (26,27), a finding attributed to the non-dichotomous airway tree structure in the canine and the inertia of the high velocity airflow during HFOV. We were somewhat surprised not to find an increase in ventilation towards the dependent base during HFOV, but this uniform ventilation distribution was seen in all of our HFOV runs (Table 2). Further study over a range of frequencies, tidal volumes, and mean airway pressures, as well as under conditions of lung injury (the typical current indication for the clinical use of HFOV), will determine the factors driving the distribution of ventilation during HFOV. If it is possible to “uncouple” ventilation distribution from local lung mechanics, as is suggested here, then future management of lung injured patients could potentially exploit this phenomenon to improve gas exchange by altering ventilation distribution to better match the altered perfusion distribution of lung disease.

## CONCLUSIONS

High-resolution volumetric ventilation maps of the lung may be obtained with the 256-slice multidetector CT scanner during both conventional and high-frequency ventilation. There is a marked difference, apparent from the ventilation maps, in the distribution of regional ventilation between CV and HFOV modes, with a significant gravitational ventilation gradient in CV that was not present during HFOV. This difference in ventilation heterogeneity was not explained by differences in regional aeration. Future more detailed studies are required to determine the factors driving the distribution of regional ventilation during HFOV and whether this phenomenon can be exploited to improve the clinical application of HFOV.

## ACKNOWLEDGMENTS

The authors would like to thank the Toshiba America Medical System CT team, particularly Rich Mather and Chloe Steveson, for access to the experimental 256 slice scanner and technical support. Dr. Eric Hoffman of the University of Iowa Comprehensive Lung Imaging Center provided the analysis software. In addition, we thank Tim Burman for his expert technical support in the laboratory.

Supported by NIH HL64368 and HL073994, and the Foundation for Anesthesia Education and Research Mentored Research Training Scientist Grant (RBE)

## REFERENCES

1. Hoffman EA, Simon BA, McLennan G. State of the Art. A structural and functional assessment of the lung via multidetector-row computed tomography: phenotyping chronic obstructive pulmonary disease. Proc Am Thorac Soc 2006;3:519–532. [PubMed: 16921136]
2. Simon BA, Christensen GE, Low DA, et al. Computed tomography studies of lung mechanics. Proceedings of the American Thoracic Society 2005;2:517–521. 506–517. [PubMed: 16352757]
3. Krishnan JA, Brower RG. High-frequency ventilation for acute lung injury and ARDS. Chest 2000;118:795–807. [PubMed: 10988205]
4. Hager DN, Fessler HE, Kaczka DW, et al. Tidal volume delivery during high-frequency oscillatory ventilation in adults with acute respiratory distress syndrome. Crit Care Med 2007;35:1522–1529. [PubMed: 17440422]
5. Chon D, Simon BA, Beck KC, et al. Differences in regional wash-in and wash-out time constants for xenon-CT ventilation studies. Respir Physiol Neurobiol 2005;148:65–83. [PubMed: 16061426]

6. Marcucci C, Nyhan D, Simon BA. Distribution of pulmonary ventilation using Xe-enhanced computed tomography in prone and supine dogs. J Appl Physiol 2001;90:421–430. [PubMed: 11160037]
7. Simon BA, Mitzner W. Design and calibration of a high-frequency oscillatory ventilator. IEEE Trans. Biomed. Eng 1991;38:214–218. [PubMed: 2066132]
8. Fuld MK, Easley RB, Saba OI, et al. CT-measured regional specific volume change reflects regional ventilation in supine sheep. J Appl Physiol 2008;104:1177–1184. [PubMed: 18258804]
9. Treppo S, Mijailovich SM, Venegas JG. Contributions of pulmonary perfusion and ventilation to heterogeneity in V(A)/Q measured by PET. J Appl Physiol 1997;82:1163–1176. [PubMed: 9104853]
10. Hoffman EA, Sinak LJ, Robb RA, et al. Noninvasive quantitative imaging of shape and volume of lungs. J Appl Physiol 1983;54:1414–1421. [PubMed: 6863100]
11. Hoffman EA. Effect of body orientation on regional lung expansion: a computed tomographic approach. JAP 1985;59:468–480.
12. Hoffman EA, Ritman EL. Invariant total heart volume in the intact thorax. Am J Physiol 1985;249:H883–890. [PubMed: 4051023]
13. Hoffman EA, Ritman EL. Heart-lung interaction: effect on regional lung air content and total heart volume. Ann Biomed Eng 1987;15:241–257. [PubMed: 3662146]
14. Liu YH, Hoffman EA, Ritman EL. Measurement of three-dimensional anatomy and function of pulmonary arteries with high-speed x-ray computed tomography. Invest Radiol 1987;22:28–36. [PubMed: 3102399]
15. Hoffman EA, Chon D. Computed tomography studies of lung ventilation and perfusion. Proc Am Thorac Soc 2005;2:492–498. 506. [PubMed: 16352755]
16. Simon BA. Regional ventilation and lung mechanics using X-ray CT. Acad Radiol 2005;12:1414–1422. [PubMed: 16253853]
17. Chon D, Beck KC, Simon BA, et al. Effect of low-xenon and krypton supplementation on signal/noise of regional CT-based ventilation measurements. J Appl Physiol 2007;102:1535–1544. [PubMed: 17122371]
18. Chon D, Beck KC, Larsen RL, et al. Regional pulmonary blood flow in dogs by 4D-X-ray CT. J Appl Physiol 2006;101:1451–1465. [PubMed: 16825517]
19. Uppaluri R, Mitsa T, Sonka M, et al. Quantification of pulmonary emphysema from lung computed tomography images. Am J Respir Crit Care Med 1997;156:248–254. [PubMed: 9230756]
20. Uppaluri R, Hoffman EA, Sonka M, et al. Computer recognition of regional lung disease patterns. Am J Respir Crit Care Med 1999;160:648–654. [PubMed: 10430742]
21. Hoffman EA, Clough AV, Christensen GE, et al. The comprehensive imaging-based analysis of the lung: a forum for team science. Acad Radiol 2004;11:1370–1380. [PubMed: 15596375]
22. Simon BA, Marcucci C, Fung M, et al. Parameter estimation and confidence intervals for Xe-CT ventilation studies: a Monte Carlo approach. JAP 1998;84:709–716.
23. Hubmayr RD, Rodarte JR, Walters BJ, et al. Regional ventilation during spontaneous breathing and mechanical ventilation in dogs. JAP 1987;63:2467–2475.
24. Robertson HT, Glenny RW, Stanford D, et al. High-resolution maps of regional ventilation utilizing inhaled fluorescent microspheres. JAP 1997;82:943–953.
25. Yamada Y, Burnham C, Hales CA, et al. Regional mapping of gas transport during high-frequency and conventional ventilation. Journal of Applied Physiology 1989;66:1209–1218. [PubMed: 2708245]
26. Allen JL, Frantz ID, Fredberg JJ. Regional alveolar pressure during periodic flow. Dual manifestations of gas inertia. J Clin Invest 1985;76:620–629. [PubMed: 4031066]
27. Allen JL, Frantz ID III, Fredberg JJ. Heterogeneity of mean alveolar pressure during high-frequency oscillations. Journal of Applied Physiology 1987;1987:223–228. [PubMed: 3558183]

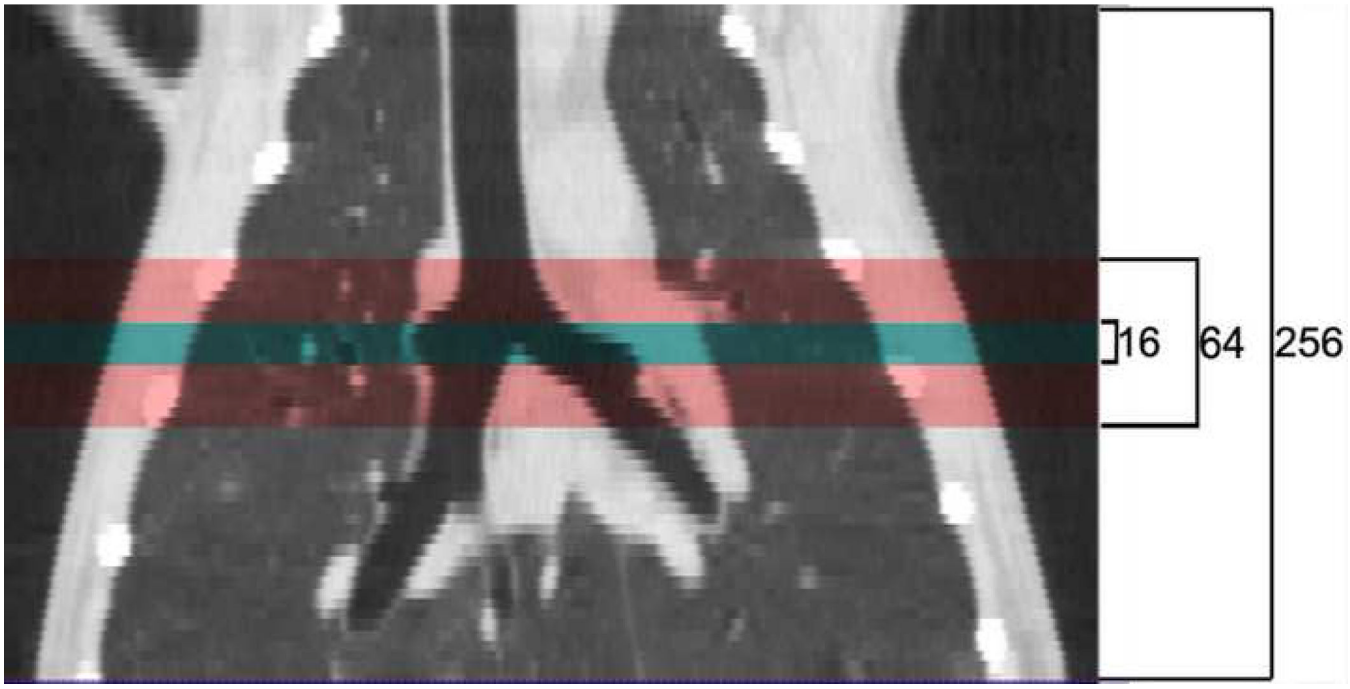


**Figure 1.**
Coronal view of the lung demonstrating the increased axial coverage of a single image acquisition with increasing number of detectors from 16 to 64 to 256.

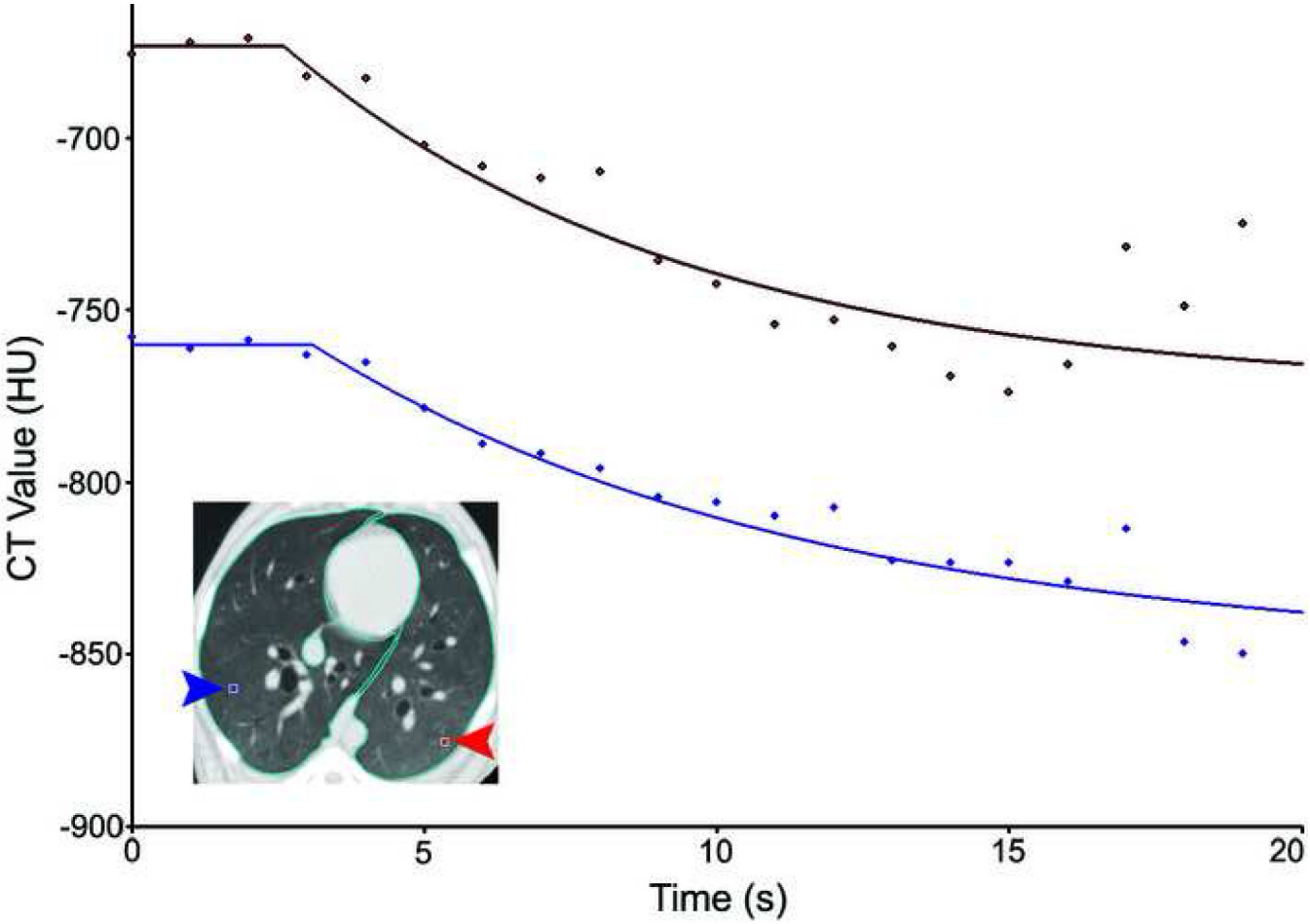


**Figure 2.**
Representative density-time curves and exponential fits for 2 regions of interest from the multibreath washout of Xe from the lung during HFOV.

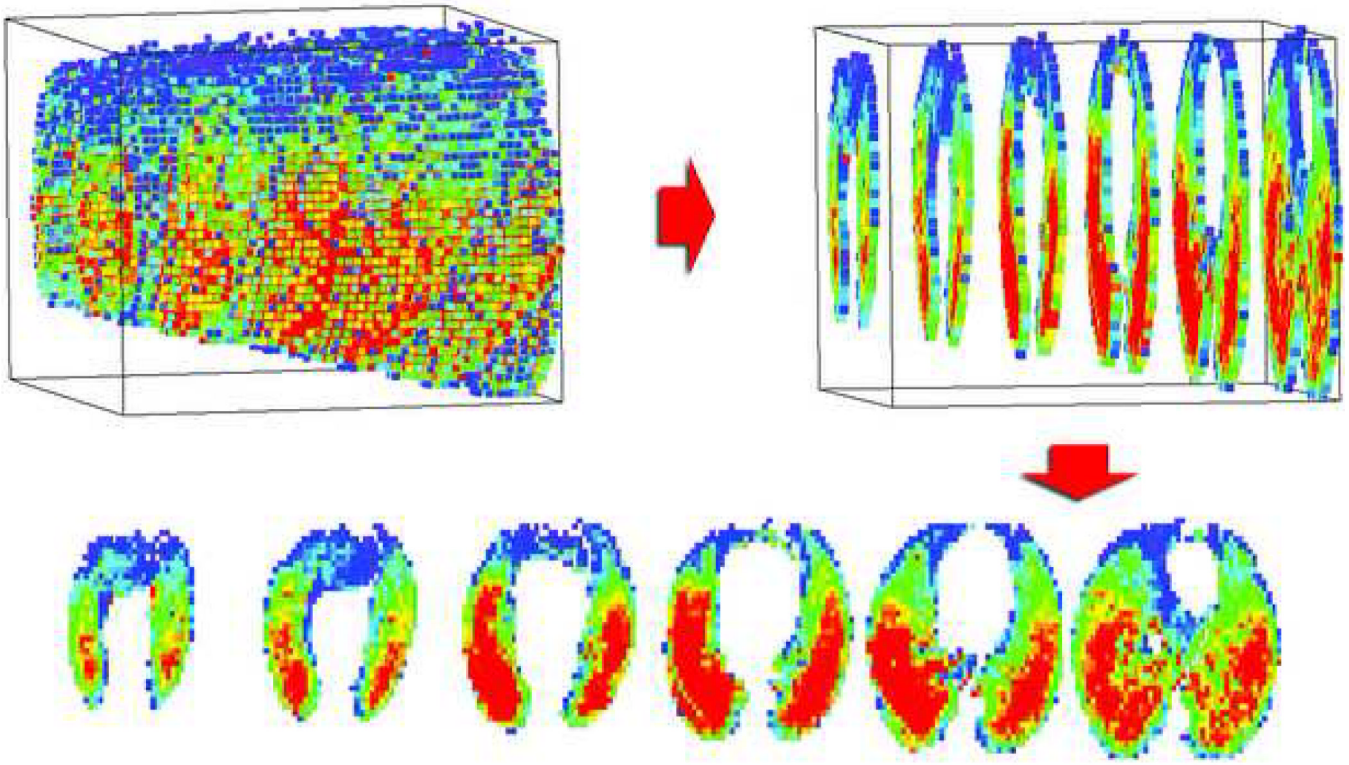

**Figure 3.**
Representation of 3-D data. Each ROI in the lung volume was separately curve fit to determine its specific ventilation and the values color-coded. For display purposes, data within each 1.8 cm of z-coverage were averaged into one 2-D colormap, creating six 2-D maps that represent the entire scanned volume from apex to base.

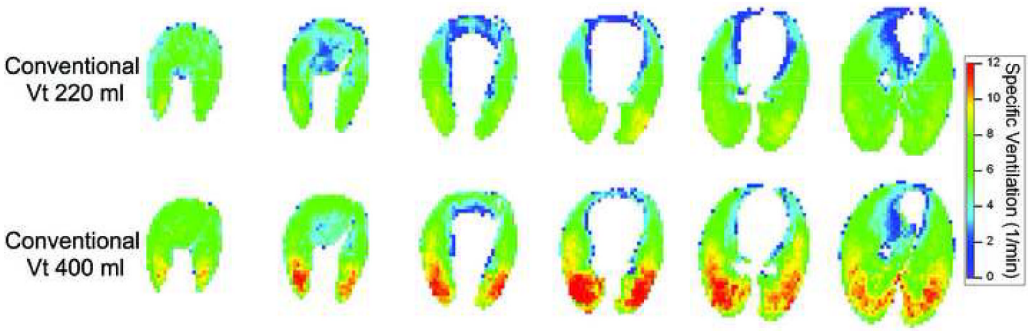


**Figure 4.**

Colormaps showing the apex to base distribution of sV̇ in subject 2 at tidal volumes of 220 and 400 ml, rate 30 breaths/minute, and 7.5 cm $H_2O$ PEEP. Note the overall increase in ventilation at the higher Vt as well as the strong vertical gradient in sV̇ seen during CV.

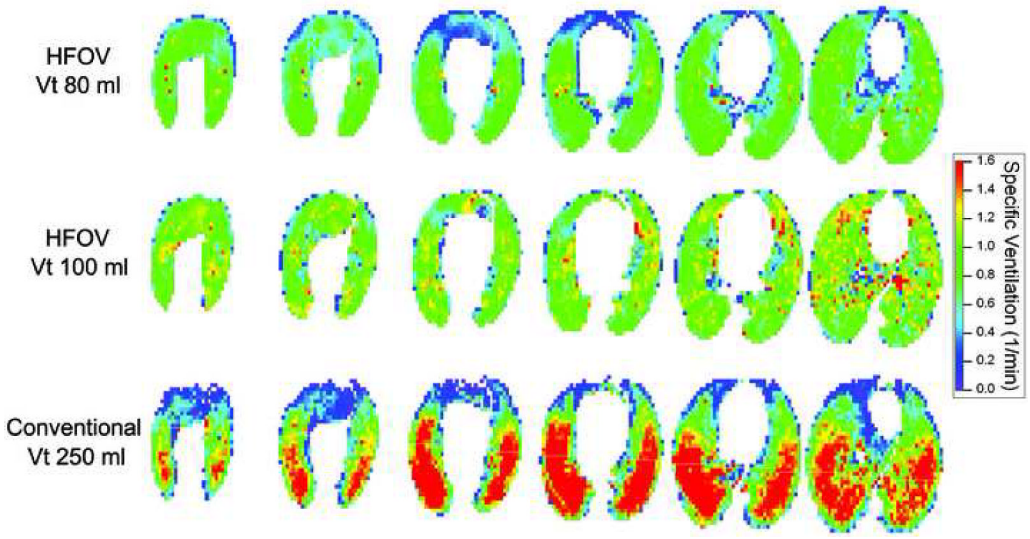


**Figure 5.**

Colormaps showing the apex to base distribution of sV̇ in subject 3 during CV at 30 breaths/min, Vt=250ml, and PEEP 7.5 cm $H_2O$, and during HFOV at frequency 10 Hz, MAP 10 cm $H_2O$, and Vt of 80 and 100 ml. There is an overall increase in sV̇ during HFOV as Vt increases. As in Figure 4, there is a steep vertical ventilation gradient during CV, but ventilation is extremely uniform during HFOV.

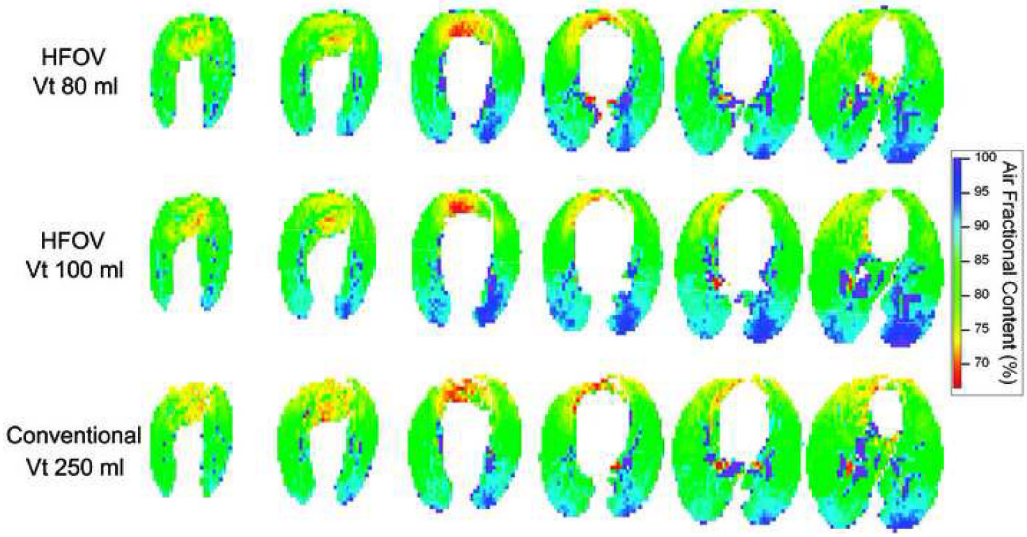


**Figure 6.**
Colormaps of lung density, expressed as % air content, for the same lung slices depicted in Figure 5. The vertical gradient in lung aeration or regional expansion is very similar during CV and HFOV.

**Table 1**

Ventilator settings. Each animal was imaged at a total of three HFOV and/or CV ventilator settings.

| Subject | Conventional Ventilation | | | High-frequency Ventilation | | |
|---|---|---|---|---|---|---|
| | RR (breaths/min) | Vt (ml) | PEEP (cm $H_2O$) | *f* (Hz) | Vt (ml) | MAP (cm $H_2O$) |
| 1 | | | | 10 | 60 | 10 |
| | | | | 10 | 80 | 10 |
| | | | | 10 | 100 | 10 |
| 2 | 30 | 220 | 7.5 | | | |
| | 30 | 400 | 7.5 | | | |
| | 30 | 400 | 0 | | | |
| 3 | 30 | 250 | 7.5 | | | |
| | | | | 10 | 80 | 10 |
| | | | | 10 | 100 | 10 |

## Table 2

Measures of Ventilation Heterogeneity

| Stepwise Linear Regression $R^2$ | HFOV | CV |
|---|---|---|
| Y | 0.028 ± 0.03 | 0.294 ± 0.12 |
| Y/Z | 0.040 ± 0.02 | 0.296 ± 0.12 |
| Y/Z/S | 0.042 ± 0.02 | 0.298 ± 0.12 |

means±SD for $R^2$; n=5 HFOV, n=4 CV. *Y*, height; *S*, side (left vs. right); *Z*, coronal location (apex-base).

| Coefficients of Variation | HFOV | CV |
|---|---|---|
| Total: $COV_t$ | 0.41 ± 0.06 | 0.46 ± 0.12 |
| Other: $COV_i$ | 0.40 ± 0.06 | 0.38 ± 0.12 |
| Y only: $COV_y$ | 0.09 ± 0.03 | 0.25 ± 0.04* |

means±SD; n=5 HFOV, n=4 CV. *Y*, dorsal-ventral (vertical) height

* $p<0.01$ HFOV vs. CV